Carbon dioxide migration along faults at the Illinois Basin – Decatur Project revealed using time shift analysis of seismic monitoring data

I. Bukar[1], R. Bell[1], A. H. Muggeridge[1], and S. Krevor[1]

[1]Department of Earth Science and Engineering, Imperial College London, Royal School of Mines, London, SW7 2BP, United Kingdom.

Key Points:

- 4D seismic time shift attributes reveal previously unidentified CO_2 migration be- haviour where traditional amplitude attributes could not.
- The CO_2 migrates from the injection interval, upwards along a permeable fault and re-emerges in overlying permeable reservoir units.
- This behavior has been previously theorized but not yet directly observed from a CO_2 storage site.

Abstract

Large scale geological storage of CO_2 is being deployed worldwide to reduce greenhouse gas emissions to the atmosphere. Previous modelling studies have investigated the potential for CO_2 migration along faults. We observe such migration at a commercial-scale, demonstration CO_2 storage project, including subsequent emergence of the CO_2 into overlying permeable layers. Previous attempts at interpreting the time-lapse seismic data using amplitude attributes were hindered by noise from the limited survey repeatability combined with a weak signal due to the stiffness of the rock. Here we apply an alternative interpretation of the seismic data using time shift attributes, resulting in clear plume anomalies. In addition to migrating up the fault, we observe the plume diverted by the start of injection at a neighboring project. This work provides field observations of theorized plume behaviors and demonstrates an approach to overcome challenges in interpreting seismic monitoring data for geological CO_2 storage.

Corresponding author: Idris Bukar, i.bukar21@imperial.ac.uk

1 Introduction

Carbon capture and geological storage is being scaled up worldwide to achieve net zero carbon emissions by 2050 (Krevor et al., 2023; Pörtner et al., 2022). Monitoring CO_2 storage through time-lapse seismic techniques has provided observations of the flow and trapping behavior of the injected CO_2 at storage projects around the world (Furre et al., 2017; Hansen et al., 2013; Ivandic et al., 2015; Roach & White, 2018). The observations have revealed fluid dynamics which are more complex and dynamic than analogous subsurface fluids systems due to the properties of CO_2 as a supercritical fluid at reservoir conditions (Cavanagh & Haszeldine, 2014; Ringrose et al., 2022).

Of particular interest is the potential for CO_2 to move buoyantly upwards from a target reservoir through leakage pathways such as a fault or wellbore. This has been investigated using geological analogues, and theoretical and numerical modelling (Gasda et al., 2004; Gilmore et al., 2022; Miocic et al., 2016; Nordbotten et al., 2009, Flemisch et al., 2024). Models show that complex dynamics emerge depending on the permeabilities of fault zones relative to reservoir units, and CO_2 migration up leakage pathways can in some instances be entirely mitigated by trapping as the plume emerges in overlying permeable strata.

Despite their importance, there are no engineered settings in which the movement of CO_2 along faults has been observed. CO_2 escape from natural subsurface accumulations has been inferred to occur through faults based on geochemical and isotope measurements of carbonate deposits and travertine veins (Shipton et al., 2004; Dockrill and Shipton; 2010; Kampman et al., 2012; Jung et al., 2014; Miocic et al., 2018). Natural hydrocarbon gas leakage has also been inferred from seismic observations of gas chimneys and associated pockmark clusters on the seafloor (e.g. Gay et al., 2007; Roelofse et al., 2020).

Time-lapse seismic surveys are the industry standard for monitoring the plume dynamics, however, their acquisition and processing must be performed in a way that maximizes repeatability, which can be affected by factors such as seasonal variations and differences in acquisition geometry (Landro, 1999; Lumley, 2001; Johnston, 2013; Meunier et al., 2001; Bakulin et al., 2007). In addition, in general, land seismic surveys can suffer from significantly more noise than marine seismic surveys due to scattering by the near surface layer (Pevzner et al., 2011; Stork, 2020). In this paper, we find evidence of CO_2 migration up faults during injection at the onshore Illinois Basin – Decatur Project CO_2 storage site using time shift analysis of time-lapse 3D (i.e. 4D) vertical seismic profile (VSP) surveys. The initial interpretation approach for the 4D data was based on amplitude difference (Coueslan et al., 2014) and normalized RMS attributes (Bauer et al., 2019), but observations of the CO_2 plume were ambiguous due to weak time-lapse signals (Coueslan et al., 2013). During the post-injection phase, well logs detected an isolated finger of CO_2 in the injection well in a shallower zone than the injection interval (Zaluski & Lee, 2021) but the lack of seismic monitoring during that period meant the origins of the CO_2 could not be ascertained. The application of an amplitude agnostic, time shift analysis, reported here, reveals clear, qualitative images of a growing CO_2 plume in this interval that has arrived by migration up a previously identified fault.

2 Methods

2.1 The Illinois Basin - Decatur Project

The Illinois Basin - Decatur Project (IBDP) was a commercial-scale demonstration CO_2 sequestration project in Decatur, Illinois, USA, which stored 1 Mt of CO_2 over three years from 2011 to 2014. The projected injected the CO_2 into the Mt. Simon Sandstone at a depth of about 2100 m. The project has an injection well

(CCS1) and a monitoring well (VW1). Wells CCS2, VW2 are the injection and monitoring wells for a nearby secondary commercial project, the Illinois Industrial Carbon Capture and Storage (IL-ICCS) project. The monitoring and site characterization data from both projects have been made publicly available and provide a comprehensive dataset suitable for studying the complex behavior of CO_2 plumes in the field.

2.2 Geologic setting

The Mt. Simon sandstone is a Cambrian-age saline aquifer and is one of the major CO_2 sequestration resources in the United States. It is over 450 m thick at the Decatur site. Leetaru and Freiburg (2014) and Freiburg et al. (2014) provide a detailed depositional and diagenetic characterization of the Mt. Simon sandstone at Decatur. It is unconformably overlain by the Eau Claire Formation, which is a predominantly shale formation over 90 m thick at the Decatur site and serves as the primary caprock for the storage unit. The Mt. Simon Sandstone is subdivided into Upper, Middle and Lower units.

The most significant controls on reservoir quality in the Mt. Simon sandstone are diagenetic, with quartz cementation the most common feature. The Middle Mt. Simon is commonly referred to as the tight zone, comprising Mt. Simon C and D, with unit D having the most quartz cement in the entire Mt. Simon sandstone. The best reservoir quality occurs in the lower Mt. Simon formation, comprising units A and B, with porosities of up to 28% and permeabilities of up to 1000 mD in Unit A, and an average porosity and permeability of 22% and 200 mD. Within this unit, there is significant variation is reservoir quality as shown by the well logs. Unit A is the injection interval for the project. Several faults were interpreted by Williams-Stroud et al. (2020) to transect the middle and lower units of the Mt. Simon sandstone with some of them extending down into the Precambrian basement. Williams-Stroud et al. (2020) interpret the fault lengths to range from approximately 250 m to 1000 m, and that some of them may comprise multiple intersecting fault planes or smaller faults.

2.3 Monitoring data

The monitoring dataset at the IBDP site comprises in-well and geophysical monitoring data including time-lapse 3D VSP surveys. Repeat saturation logs recorded CO_2 saturation profiles periodically in wells CCS1 and VW1. Time-lapse 3D VSP surveying was chosen as the main geophysical monitoring technique to observe the CO_2 plume development over time. The surveys were acquired using surface vibrator sources with 3-component geophones permanently installed in a shallow geophysical monitoring well GM1 located 60 m northwest of the injection well. A monitor survey was acquired each year from 2012 to 2015 (M1-M4), with a baseline survey acquired in 2011 (B2) being the reference pre-injection survey. At the time of M1, M2, M3 and M4 surveys, 74 kt, 433 kt, 730 kt and 1 Mt of CO_2 had been injected, respectively. Analysis of the time-lapse vertical seismic profile data is the main focus of this work. The survey dates, near-surface conditions during acquisition and injected CO_2 mass are reported by Coueslan et al. (2013) and provided in the Supplementary Information.

The main processing steps performed for the 4D VSP data prior to its public release include de-noise and amplitude scaling, wavefield separation, deconvolution and pre-stack depth migration. These processing steps were carried out for each monitor alongside the baseline (B2), ensuring the extraction of co-located sources (given differences in source locations for the different surveys) and matching geometries. Details of the time-lapse co-processing are provided in the time-lapse 3D VSP processing reports (Schlumberger, 2015). We use the migrated stacks as inputs to our analysis.

2.4 Time shift attribute extraction

Previous investigations at the IBDP used amplitude attributes including NRMS and amplitude difference. Coueslan et al. (2013) presented NRMS over a zone containing the injection interval (1980 m – 2195 m) and a shallow zone (1524 m – 1980 m) covering the Middle and Upper Mt. Simon and the Eau Claire Shale primary seal. While the strongest NRMS anomalies are in the deeper zone, there are still anomalies in the shallow zone. They also show an amplitude difference section where differences can be observed outside the injection interval window (Figure 6 in Coueslan et al. (2013)). This leaves questions particularly about the finer-scale fluid movement within the entire Mt. Simon sandstone. An amplitude-based interpretation is insufficient to answer these questions. We performed an analysis of time shifts in an attempt to overcome these difficulties in interpretation.

Time shift attributes of 4D seismic data have been used successfully to monitor fluid movement in oil and gas reservoirs (Benguigui et al., 2012; Falahat et al., 2011; Santos et al., 2016) and to support amplitude interpretation at CO_2 storage sites (Arts et al., 2004; Chadwick et al., 2004, 2005; Furre et al., 2015; Grude et al., 2013). Time shifts are induced as a result of changes in fluid content or stress leading to compaction or extension in the reservoir or the overburden. Landrø and Stammeijer (2004) define the relative change in elastic wave travel time due to changes in subsurface layer thicknesses (physical strain) and velocity as $\frac{\Delta t}{t} = \frac{\Delta z}{z} - \frac{\Delta v}{v}$, where $\frac{\Delta t}{t}$ is the relative time shift or time strain, $\frac{\Delta z}{z}$ is the vertical physical strain, and $\frac{\Delta v}{v}$ is the relative velocity change, which is a function of the rock physics properties of the rock and the magnitude of the saturation change. MacBeth et al. (2020) provide a review of various time shift estimation algorithms, from the commonly used and simpler cross-correlation based methods to sophisticated waveform inversion approaches.

We implement a time shift algorithm based on the Dynamic Time Warping (DTW) algorithm of Hale (2013), modified to avoid dependency on amplitudes. Our implementation is based on matching features – peaks and troughs – between seismic traces from the baseline and monitor surveys. DTW instead attempts to match amplitudes between seismic traces, which in our case we expect to change between baseline and monitor even where there is no CO_2 present, due to the fluid effect being so subtle. The application of DTW under these circumstances therefore leads to noise. We tested this approach through synthetic modelling; we produced 1D (pseudo-2D) synthetic models based on well logs in well CCS1 (see the Supplementary Information) and used the repeat saturation logs to produce monitor synthetics under fully patchy and fully uniform mixing conditions.

The feature-based warping approach operates in a similar way to the standard DTW algorithm which is based on the minimizing the dissimilarity error between two traces:

$$e[i,q] = (f[i] - g[i+l]), \qquad (1)$$

where i is the sample index, l is the integer lag or time shift between seismic traces, and f and g are the seismic amplitudes of the baseline and monitor traces, respectively.

However, in our feature-based implementation, the objective is to align features (peaks and troughs) between two seismic traces by minimizing the geometric dissimilarity between these features. The dissimilarity error is defined as:

$$e_{feature}[i,q] = d\left(f_{feature}[i], g_{feature}[i+l]\right) \qquad (2)$$

where$f_{feature}[i]$ and $g_{feature}[i+l]$ are the positions of key features in the baseline and monitor traces, respectively, and $d\left(f_{feature}[i], g_{feature}[i+l]\right)$ is a measure of the distance between the features in the two traces, in this case the L1 or Manhattan distance. The cost matrix is filled in using the distances between the corresponding features in the baseline and monitor traces. The warping path is then optimized to minimize the cumulative feature distance along the path. Therefore, the warping is guided entirely by the spatial relationships between key features in the traces, without any consideration of the amplitudes of these features. Our synthetic modelling shows that we can detect CO_2 through feature-based warping for a 5 m thick layer at CO_2 saturation as low as 10% under uniform saturation, and for thicker layers under fully patchy saturation (see Supplementary Information). Our synthetic modelling also, however, reveals that the apparent thickness of CO_2 one would recover from seismic data is much thicker than the true thickness. This is expected given the low-frequency nature of seismic data.

Time shifts were extracted from full stacks of each of the four 3D monitor surveys relative to the B2 baseline survey. We extract time shifts starting from 870 ms (or about 1500 m), because data folds are minimum in the shallow interval due to VSP geometry constraints. The time-lapse 3D VSP processing report notes that data shallower than 1500 m was not used to compute time-lapse attributes for the same reason (Schlumberger, 2015). We obtain time strain by taking the first derivative of the time shift volumes.

3 Results and Discussion

3.1 CO_2 plume interpretation from relative velocity change

We interpret CO_2 plumes qualitatively from the results of time strain, identifying multiple plume layers, with the feature having the greatest areal extent being in the deepest in the injection interval (the lower unit of the Mt. Simon A formation). Figure 1 shows views of the plume features in the shallowest interval for all four monitors. These features are generally consistent across time from 2012 to 2015. We interpret the regions of relative velocity change < -0.02 to be areas of CO_2 accumulation. Also shown are four out of several faults interpreted by Williams-Stroud et al. (2020). These faults were interpreted prior to injection, from 3D surface seismic data acquired during site characterization. Some of the interpreted plume anomalies exceed the lateral coverage of the 3D VSP cubes.

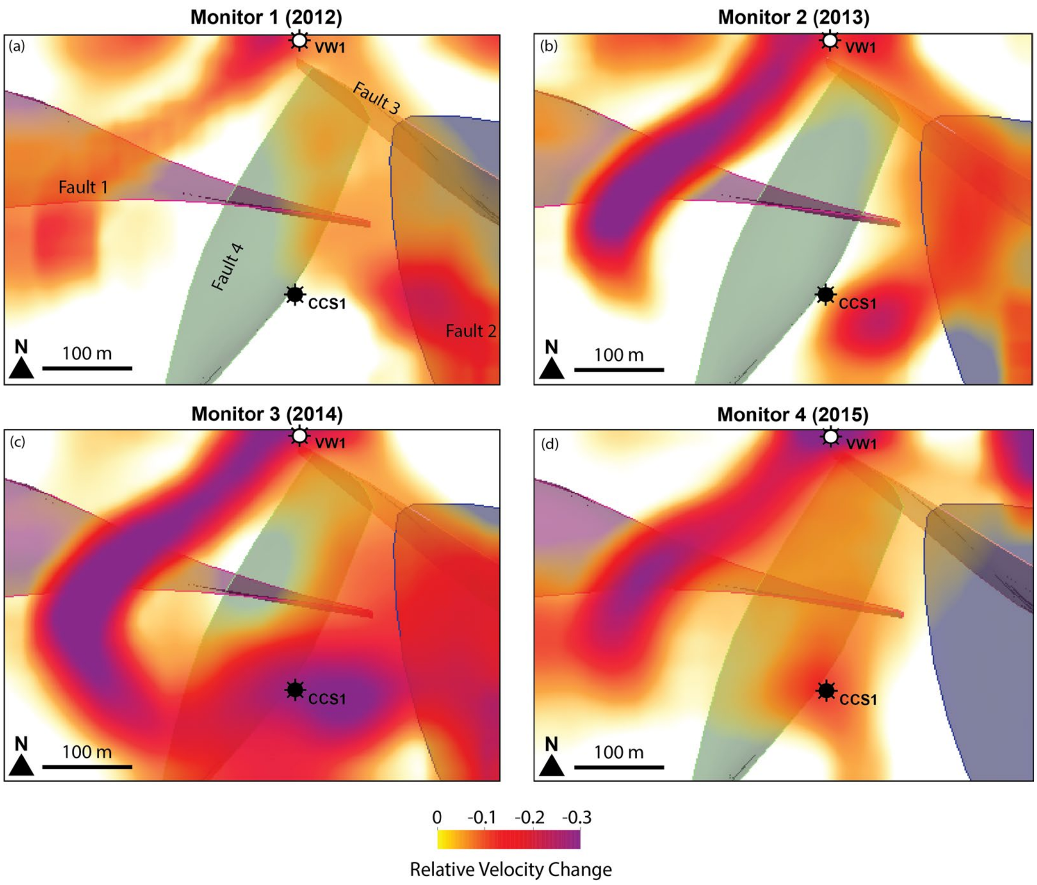

Figure 1. Map views of relative velocity change showing the shallowest layer (at about 1550 m) from all four monitors (M1-M4) relative to the baseline (B2). Note the excellent consistency in the features.

The similarity and consistency in the geometry of the plume features across the monitors suggests that the vertical distribution behavior developed quite early, within four months of injection (the time of the first monitor). Therefore, with increasing mass of injected CO_2 over time, we expect any major growth of the plumes to be lateral, which the narrow seismic cubes make impossible to fully observe.

Although we do not attempt to invert for CO_2 saturation given uncertainty in the fluid mixing type, we note that our ranges of relative velocity change can be higher in terms of absolute values than the maximum expected from fluid substitution modelling. This is attributed to data quality leading to errors in the time shift estimation. Because time strain and therefore relative velocity change is a derivative of time shift, even a small error in time shift will magnify when converted to relative velocity change (Macbeth and Izadian, 2023).

3.2 Capillary barriers and fault zone migration of CO_2 within the Mt. Simon

We interpret fault zone migration of CO_2 in the Mt. Simon sandstone. We infer such migration form areas of multiple plume features separated by low reservoir quality zones, with the plume features intersected by a fault. Figure 2 (a) shows such a scenario in the south-eastern corner of the cube. All three shallower layers appear to have emerged through Fault 2 from the injection interval. We interpret that CO_2 from the injection interval preferentially flows upwards under buoyancy through the fault zone and emerges at shallower intervals.

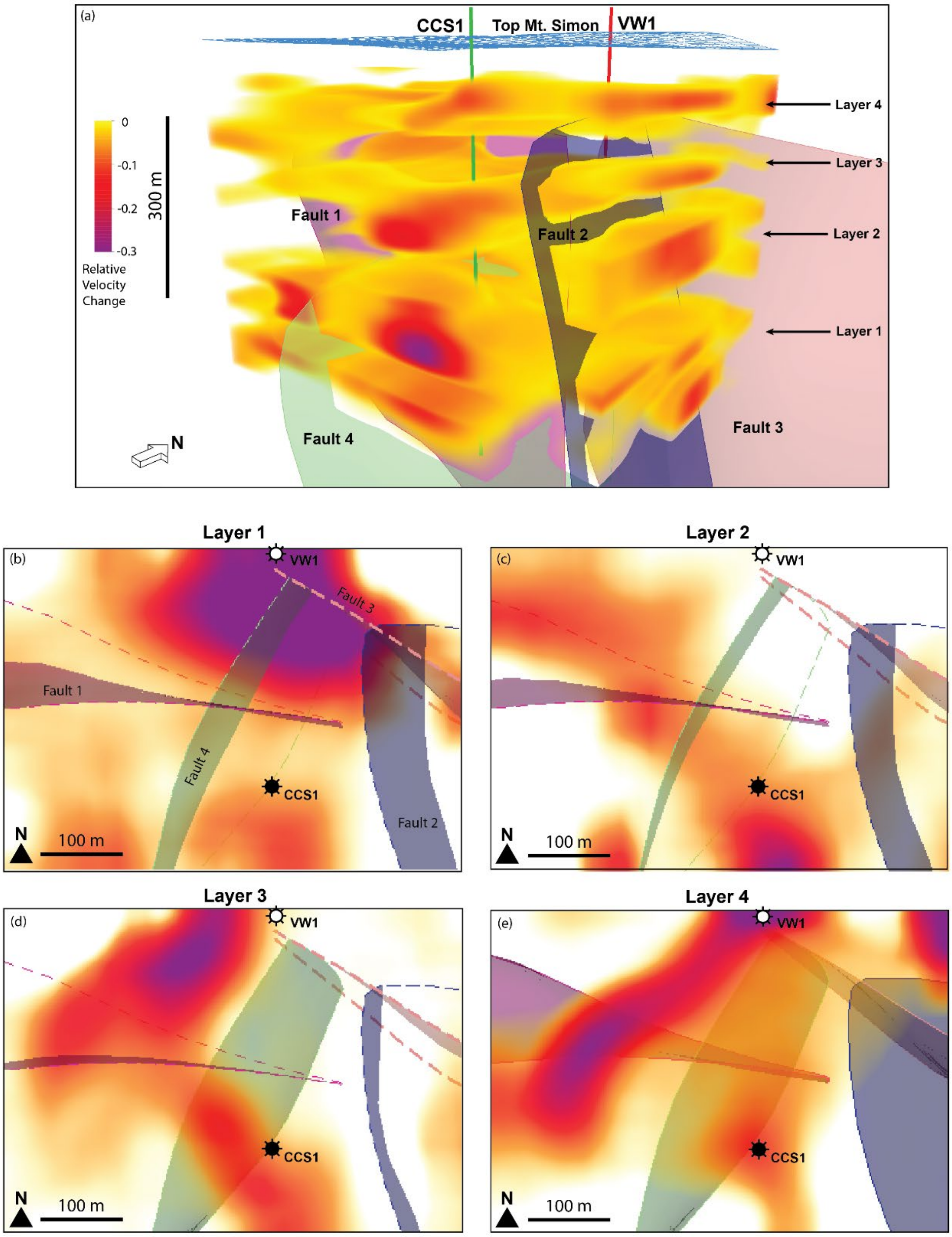

Figure 2. (a) A 3D view of relative velocity change for M4 relative to B2. Our interpretation is that regions where the relative change in velocity is < – 0.02 are regions of CO2 saturation. Also shown are three out of several faults interpreted by Williams-Stroud et al. (2020). Here we identify four layers or zones with CO2 accumulations. (b) Map views of the four identified layers of CO2 from Layer 1 to 4.

The vertical and lateral distributions of the plumes appear to be controlled by reservoir quality. We validate this by comparing observations of saturation distribution and reservoir quality in the wells and in seismic data. As shown in Figure 3, well log panels for the injection and monitoring wells show the variation in reservoir quality across the Mt. Simon. Repeat saturation logging measurements are shown from each year across the CCS1 injection period through to post-injection and to the CCS2 injection period. From observation of the time-lapse saturation logs, it can be interpreted that the injected CO_2 preferentially fills the high-quality reservoir sandstones and avoids poorer quality or tight sandstones (Figure 3 (a)). We define tight sandstones as those with low porosity, low permeability and high capillary entry pressure.

Early modelling attempts at the Decatur site evaluated the risk of extensive lateral migration as low and expected a more vertical filling of the lower Mt. Simon sandstone by the injected CO_2 (Finley et al., 2013). This informed the design of the time-lapse VSP surveys used for studying the plume development (Coueslan et al., 2009). Strandli and Benson (2013) and Strandli et al. (2014) show that there is excellent pressure communication between the two zones where the fingers of the plume are detected in VW1 (zones 2 and 3 in Figure 3 (a)), with both bottomhole pressure gauges showing identical behaviors and near-instantaneous responses to varying injection rates. Nonetheless, the lower finger does not at any point buoyantly rise and coalesce with the upper finger, even after injection had ceased, as it is held back by a tight zone at 1920 m (Figure 3 (a)). The upper finger is also contained by another tight zone at 1905 m. These tight zones clearly have sufficient permeability to allow good pressure communication across and even allow the flow of displaced brine as shown by Strandli et al. (2014). This suggests that these tight zones are capillary barriers rather than permeability barriers.

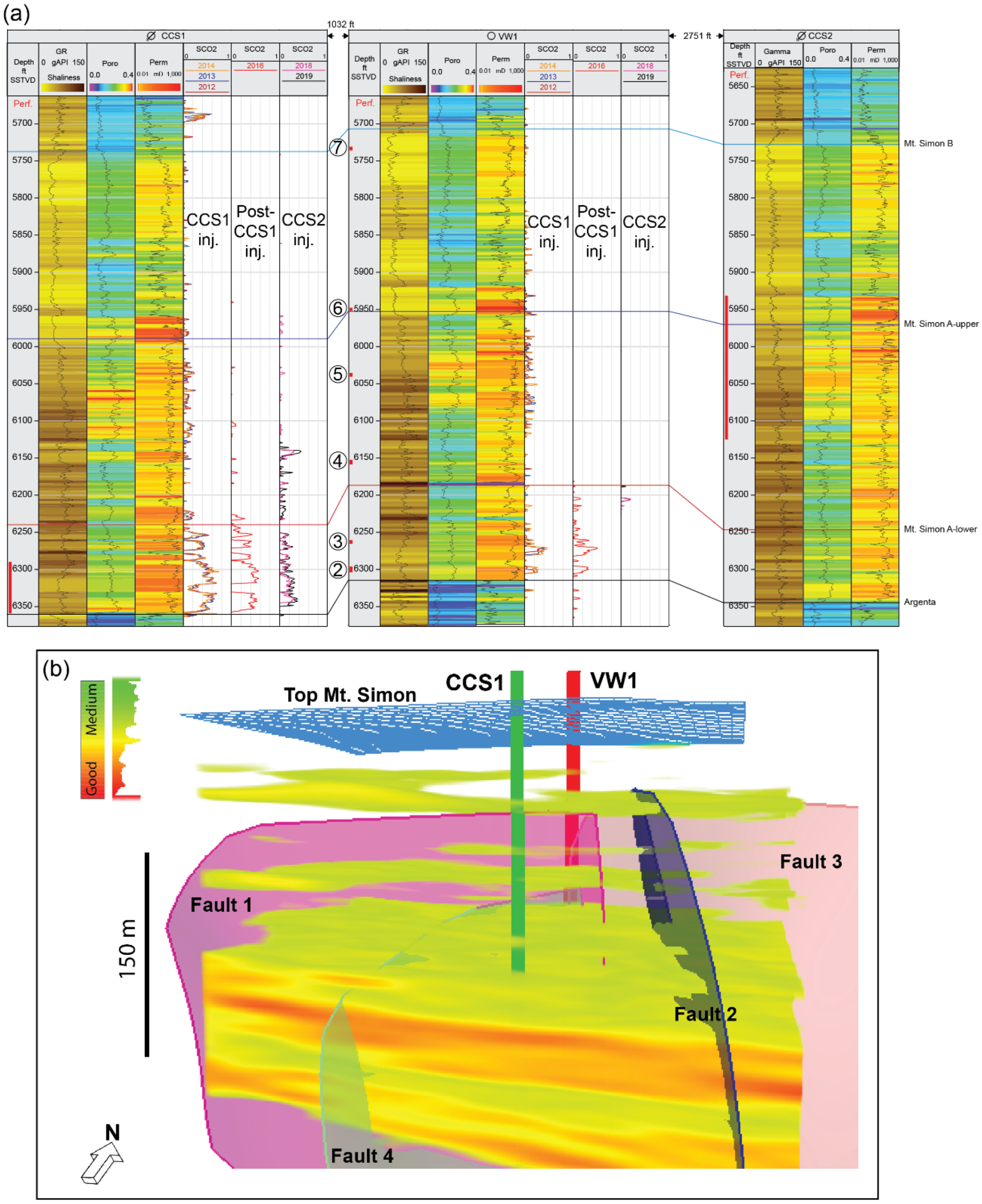

Figure 3. (a) Well log panels for the injection and monitoring wells showing the variation in reservoir quality across the Mt. Simon in terms of shaliness, porosity and permeability. Repeat saturation logging measurements are shown form each year across the CCS1 injection period through to post-injection and to the CCS2 injection period. Perforated zones are shown in red. Pressure monitoring zones are numbered. (b) Reservoir quality represented by acoustic impedance in 3D, with low quality zones rendered transparent.

Away from the wells, we use a 3D volume of acoustic impedance, a product of rock bulk density and P-wave velocity, to represent reservoir quality. The acoustic impedance 3D volume was released as part of the IBDP dataset. Zones of high acoustic impedance represent low quality or tight zones and vice-versa. The acoustic impedance volume was derived from inversion of 3D seismic data acquired for site characterization. Acoustic impedance is a good proxy for reservoir quality in this case because the primary cause of poor reservoir quality in the Mt. Simon is quartz cementation (Freiburg et al., 2014), which typically results in higher P-wave velocities by stiffening the rock frame. Cementation also means porosity destruction, which raises rock bulk densities. The acoustic impedance volume shown in Figure 3 (b) shows the absence of high-quality pathways through the rock matrix for CO_2 to migrate upwards from the injection interval.

The behavior of CO_2 emergence in a high-quality zone could mitigate leakage up conductive faults as the amount of CO_2 that continues to migrate up a fault is progressively reduced with each encountered high-quality zone. Where the conductive faults are intra-reservoir and do not traverse the seal, they would merely serve to provide access to other good quality zones of the reservoir, distributing the CO_2 among them, as has been shown through modelling (Yang et al., 2018; Zhang et al., 2024). Such is the case at Decatur; the fault provides flow pathways to overlying good quality zone and stringers in the Mt. Simon formation, which the injected CO_2 is unable to access normally due to capillary barriers.

3.3 Origins of late CO_2 arrival at injection well post-injection

An isolated finger of CO_2 was detected in the injection well during the post-injection period of the project in May 2018. This CO_2 was detected in the upper unit of the Mt. Simon A formation, and it increased in saturation in the March 2019 survey (Figure 3(a)). The saturation logging report (Swager, 2019) suggested the origins of the CO_2 to be the Illinois Industrial Carbon Capture and Storage (IL-ICCS) project located about 1100 m north of well CCS1. The injection well at this secondary project, well CCS2, had been injecting into the upper unit of the Mt. Simon A formation for 13 months at the time of detection. A simplified mass and volume balance analysis shows it is unlikely that enough CO_2 had been injected in well CCS2 to have reached well CCS1 at the time of detection. In addition, the uppermost part of the A-Upper unit (c. 1814 m in well CCS2) has the highest reservoir quality throughout the entire Mt. Simon sandstone, with permeabilities up to 1000 mD. Given the excellent correlation of this interval across the three wells, it is the most likely pathway for any rapid migration of CO_2. However, the late-arriving CO_2 was detected instead in an interval in the lower half of the unit at a depth of 1875 m. This interval is deeper than the injection zone in CCS2, which would require the CO_2 to flow downdip. This is unlikely outside the viscous region due to buoyancy forces. Moreover, no CO_2 was detected in the corresponding interval of well VW1, which is located between wells CCS2 and CCS1. Figure S.4 in the Supplementary Information summarizes this analysis.

We present an alternative hypothesis based on plume interpretations from 4D seismic time shift analysis and pressure and saturation logging data. We propose that the CO_2 instead originated from the CCS1 well – the same well it was detected in – but from layer 1 in the underlying injection interval. The evidence supports that the CO_2 travelled vertically through Fault 2, forming layer 2 (Figure 2 (c)). Over time, layer 2 got larger as more CO_2 pooled. Once injection began at the nearby IL-ICCS project, the pressure gradient induced as a result of active CO_2 injection in well CCS2 then forces layer 2 to flow across the face of CCS1, resulting in this new detection. We argue this given that bottomhole pressure data shows good pressure communication between wells CCS1 and CCS2. Our interpretation of the overall CO_2 migration behavior during the three stages of CCS1 injection, post CCS1 injection and

CCS2 injection is summarized in Figure 4.

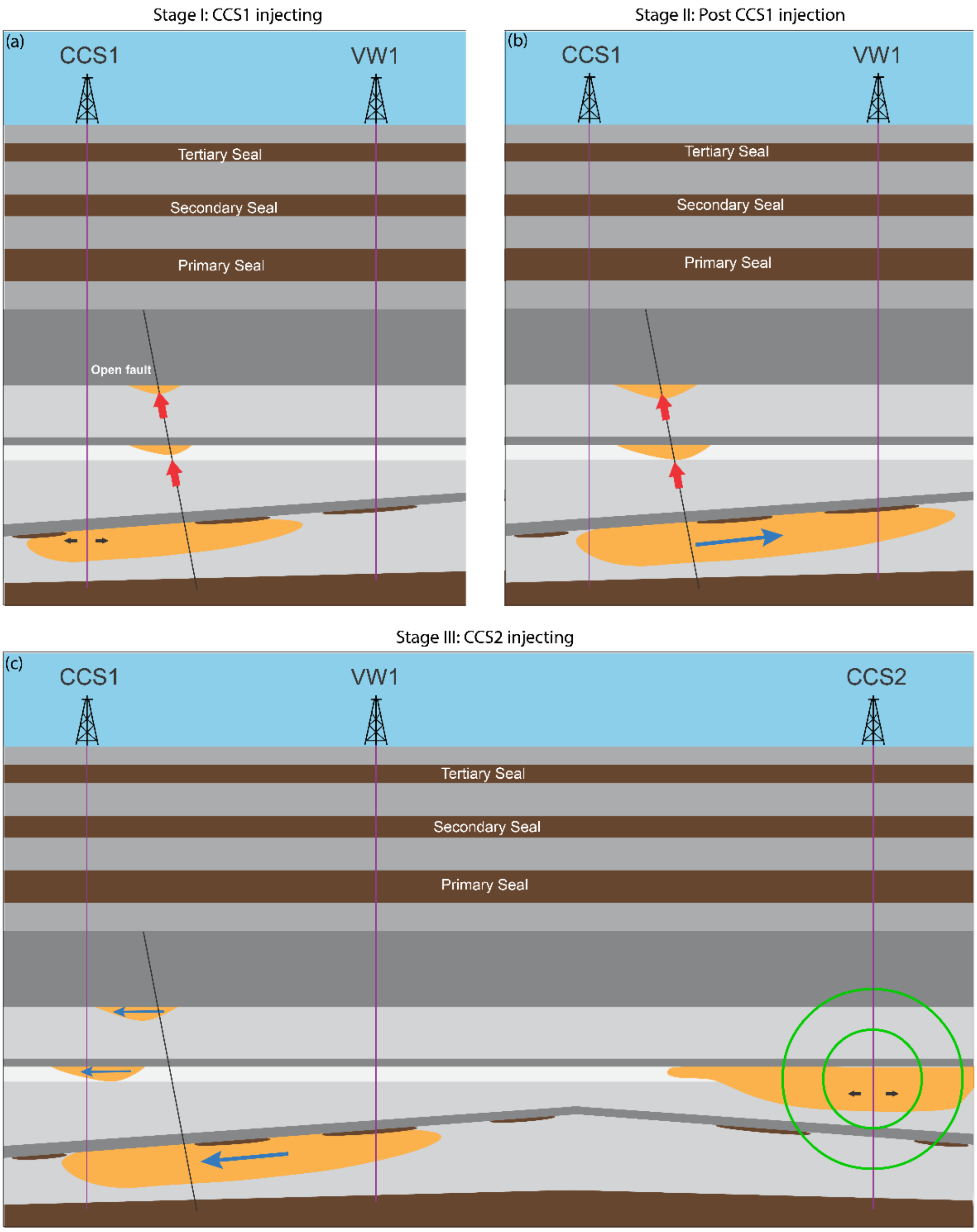

Figure 4. A conceptual schematic summarizing the overall plume behavior during (a) CCS injection, (b) post CCS1 injection, and (c) CCS2 injection. Reservoir quality is indicated in grayscale with darker tones representing tight zones.

4 Conclusion

We have re-interpreted data from time-lapse seismic surveys at the Illinois Basin - Decatur Project and shown that the CO_2 plume had been migrating along major faults between high quality units of the reservoir and moving laterally in response to injection at a neighboring site. The analysis provides an important dataset of previously theorized plume migration behavior between fault zones and reservoir units. This interpretation was otherwise not possible using a conventional analysis of amplitude attributes. The factors which hindered a more straightforward amplitude-based analysis may occur commonly in projects, especially in onshore settings. The much clearer picture of CO_2 plume anomalies provided by time shifts allowed a meaningful integration of multiple independent measurements to produce a coherent interpretation of the migration behavior of injected CO_2 at the Decatur site. We were able to identify an interplay of capillary heterogeneity and upward flow of CO_2 along permeable faults under buoyancy forces. In addition, we identify the role of pressure gradients resulting from CO_2 injection at a neighboring project in causing the re-mobilization and flow of CO_2 at the Decatur project post-injection. These behaviors and their impacts have been previously theorized, and the observations provided from an industry scale geological CO_2 storage site provides important validation of these theories and data from which future projects may be designed.

Acknowledgments

The authors wish to acknowledge support from SLB and Ikon Science for academic licenses for Petrel and RokDoc. We thank the Petroleum Technology Development Fund for providing the funding for this research.

Open Research

The original dataset and reports used in this study were made publicly available by the National Energy Technology Laboratory through the Energy Data eXchange (ISGS, 2021a, 2021b). Bukar, 2024 provides the processed data and code used in this study. The codes are also accessible at https://github.com/ImperialCollegeLondon/4d-seismic-co2

References

Arts, R., Eiken, O., Chadwick, A., Zweigel, P., Van der Meer, L., & Zinszner, B. (2004). Monitoring of CO_2 injected at Sleipner using time-lapse seismic data [Publisher: Elsevier]. *Energy*, *29* (9-10), 1383–1392. https://doi.org/10.1016/j.energy.2004.03.072

Bakulin, A., Lopez, J., Herhold, I. S., & Mateeva, A. (2007). Onshore monitoring with virtual-source seismic in horizontal wells: Challenges and solutions. In SEG Technical Program Expanded Abstracts 2007 (pp. 2893-2897). Society of Exploration Geophysicists. https://doi.org/10.1190/1.2793067

Bauer, R., Will, R., Greenberg, S. E., & Whittaker, S. G. (2019). Illinois basin–Decatur project. In *Geophysics and geosequestration* (pp. 339–369). Cambridge University Press. https://doi.org/10.1017/9781316480724.020

Benguigui, A., Roberts, G., & Shaw-Champion, M. (2012). Time-lapse 2D seismic steam- flood monitoring-a case study from offshore republic of Congo, the Emeraude field. *74th EAGE Conference and Exhibition incorporating EUROPEC 2012*, cp–293. https://doi.org/10.3997/2214-4609.20148837

Brie, A., Pampuri, F., Marsala, A., & Meazza, O. (1995). Shear sonic interpretation in gas-bearing sands. *SPE Annual Technical Conference and*

Exhibition, SPE–30595. https://doi.org/10.2118/30595-MS

Bukar, Idris. (2024). ImperialCollegeLondon/4d-seismic-co2: v0.0 (pre-release). [Software]. Zenodo. https://doi.org/10.5281/zenodo.11165813

Caspari, E., Müller, T. M., & Gurevich, B. (2011). Time-lapse sonic logs reveal patchy CO_2 saturation in-situ. *Geophysical Research Letters*, *38* (13). https://doi.org/10.1029/2011GL046959

Cavanagh, A. J., & Haszeldine, S. (2014). The Sleipner storage site: Capillary flow modeling of a layered CO_2 plume requires fractured shale barriers within the Utsira Formation [Publisher: Elsevier]. *International Journal of Greenhouse Gas Control*, *21*, 101–112. https://doi.org/10.1016/j.ijggc.2013.11.017

Chadwick, R., Arts, R., & Eiken, O. (2005). 4D seismic quantification of a growing CO_2 plume at Sleipner, North Sea [Issue: 1]. *Geological Society, London, Petroleum Geology Conference series*, *6*, 1385–1399. https://doi.org/10.1144/0061385

Chadwick, R., Arts, R., Eiken, O., Kirby, G., Lindeberg, E., & Zweigel, P. (2004). 4D seismic imaging of an injected CO_2 plume at the Sleipner Field, Central North Sea [Publisher: The Geological Society of London]. *Geological Society, London, Memoirs*, *29* (1), 311–320. https://doi.org/10.1144/gsl.mem.2004.029.01.29

Coueslan, M. L., Ali, S., Campbell, A., Nutt, W., Leaney, W., Finley, R., & Greenberg, S. (2013). Monitoring CO_2 injection for carbon capture and storage using time- lapse 3D VSPs [Publisher: Society of Exploration Geophysicists]. *The Leading Edge*, *32* (10), 1268–1276. https://doi.org/10.1190/tle32101268.1

Coueslan, M. L., Butsch, R., Will, R., & Locke II, R. A. (2014). Integrated reservoir monitoring at the Illinois Basin–Decatur Project [Publisher: Elsevier]. *Energy*

Procedia, *63*, 2836–2847. https://doi.org/10.1016/j.egypro.2014.11.306

Coueslan, M. L., Leetaru, H. E., Brice, T., Leaney, W. S., & McBride, J. H. (2009). Designing a seismic program for an industrial CCS site: Trials and tribulations [Publisher: Elsevier]. *Energy Procedia*, 1 (1), 2193–2200. https://doi.org/10.1016/j.egypro.2009.01.285

Dockrill, B., & Shipton, Z. K. (2010). Structural controls on leakage from a natural CO_2 geologic storage site: Central Utah, USA. *Journal of Structural Geology*, *32* (11), 1768– 1782. https://doi.org/10.1016/j.jsg.2010.01.007

Falahat, R., Shams, A., & MacBeth, C. (2011). Towards quantitative evaluation of gas injection using time-lapse seismic data [Publisher: European Association of Geoscientists & Engineers]. *Geophysical Prospecting*, *59* (2), 310–322. https://doi.org/10.1111/j.1365-2478.2010.00925.x

Faulkner, D., Jackson, C., Lunn, R., Schlische, R., Shipton, Z., Wibberley, C., & Withjack, M. (2010). A review of recent developments concerning the structure, mechanics and fluid flow properties of fault zones. *Journal of Structural Geology*, *32* (11), 1557– 1575. https://doi.org/10.1016/j.jsg.2010.06.009

Finley, R. J., Frailey, S. M., Leetaru, H. E., Senel, O., Cou¨eslan, M. L., & Scott, M. (2013). Early operational experience at a one-million tonne CCS demonstration project, Decatur, Illinois, USA [Publisher: Elsevier]. *Energy Procedia*, *37*, 6149–6155. https://doi.org/10.1016/j.egypro.2013.06.544

Flemisch, B., Nordbotten, J. M., Fernø, M., Juanes, R., Both, J. W., Class, H., et al., (2024). The FluidFlower validation benchmark study for the storage of CO_2. Transport in Porous Media, 151(5), 865-912. https://doi.org/10.1007/s11242-023-01977-7

Freiburg, J., Morse, D. G., Leetaru, H. E., Hoss, R. P., & Yan, Q. (2014). A depositional and diagenetic characterization of the Mt. Simon sandstone at the Illinois Basin-Decatur Project carbon capture and storage site, Decatur, Illinois, USA [Publisher: Illinois State Geological Survey, Prairie Research Institute, University of Illinois Urbana-Champaign]. https://hdl.handle.net/2142/55338

Furre, A.-K., Eiken, O., Alnes, H., Vevatne, J. N., & Kiær, A. F. (2017). 20 years of monitoring CO_2-injection at Sleipner [Publisher: Elsevier]. *Energy procedia*, *114*, 3916– 3926. https://doi.org/10.1016/j.egypro.2017.03.1523

Furre, A.-K., Kiær, A., & Eiken, O. (2015). CO_2-induced seismic time shifts at Sleipner [Publisher: Society of Exploration Geophysicists and American Association of Petroleum Geologists]. *Interpretation*, *3* (3), SS23–SS35. https://doi.org/10.1190/INT-2014-0225.1

Gasda, S. E., Bachu, S., & Celia, M. A. (2004). Spatial characterization of the location of potentially leaky wells penetrating a deep saline aquifer in a mature sedimentary basin. *Environmental geology*, *46*, 707–720. https://doi.org/10.1007/s00254-004-1073-5

Gassmann, F. (1951). Über die elastizität poröser medien: Vierteljahrss-chrift der Naturforschenden Gesellschaft in Zurich, vol. 96. https://cir.nii.ac.jp/crid/1570291224657132800

Gay, A., Lopez, M., Berndt, C., & Séranne, M. (2007). Geological controls on focused fluid flow associated with seafloor seeps in the Lower Congo Basin. Marine and Petroleum Geology, 244, 68-92. http://doi/10.1016/j.margeo.2007.06.003

Gilmore, K. A., Sahu, C. K., Benham, G. P., Neufeld, J. A., & Bickle, M. J. (2022). Leakage dynamics of fault zones: Experimental and analytical study with application to CO_2 storage. *Journal of Fluid Mechanics*, *931*, A31. https://doi.org/10.1017/jfm.2021.970

Grude, S., Landrø, M., & Osdal, B. (2013). Time-lapse pressure–saturation discrimination for CO_2 storage at the Snøhvit field [Publisher: Elsevier]. *International Journal of Greenhouse Gas Control*, *19*, 369–378. https://doi.org/10.1016/j.ijggc.2013.09.014

Hale, D. (2013). Dynamic warping of seismic images: Geophysics, 78. *S105–S115*. https://doi.org/10.1190/geo2012-0327.1

Han, D., & Batzle, M. (2014). FLAG fluid calculator. *University of Houston Fluids/DHI Consortium*.

Hansen, O., Gilding, D., Nazarian, B., Osdal, B., Ringrose, P., Kristoffersen, J.-B., Eiken, O., & Hansen, H. (2013). Snøhvit: The history of injecting and storing 1 mt CO_2 in the fluvial tubåen fm. *Energy Procedia*, *37*, 3565–3573. https://doi.org/10.1016/j.egypro.2013.06.249

Ivandic, M., Juhlin, C., Lueth, S., Bergmann, P., Kashubin, A., Sopher, D., Ivanova, A., Baumann, G., & Henninges, J. (2015). Geophysical monitoring at the Ketzin pilot site for CO_2 storage: New insights into the plume evolution [Publisher: Elsevier]. *International Journal of Greenhouse Gas Control*, *32*, 90–105. https://doi.org/10.1016/j.ijggc.2014.10.015

Johnston, D. H. (2013). *Practical applications of time-lapse seismic data*. Society of Exploration Geophysicists. https://doi.org/10.1190/1.9781560803126

Jung, N.-H., Han, W. S., Watson, Z., Graham, J. P., & Kim, K.-Y. (2014). Fault-controlled CO_2 leakage from natural reservoirs in the Colorado Plateau, east-central Utah. *Earth and Planetary Science Letters*, *403*, 358–367. https://doi.org/10.1016/j.epsl.2014.07.012

Kampman, N., Burnside, N. M., Shipton, Z. K., Chapman, H. J., Nicholl, J. A., Ellam, R. M., & Bickle, M. J. (2012). Pulses of carbon dioxide emissions from intracrustal faults following climatic warming. Nature Geoscience, 5, 352-358. https://doi.org/10.1038/ngeo1451

Krevor, S., de Coninck, H., Gasda, S. E., Ghaleigh, N. S., de Gooyert, V., Hajibeygi, H., Juanes, R., Neufeld, J., Roberts, J. J., & Swennenhuis, F. (2023). Subsurface carbon dioxide and hydrogen storage for a sustainable energy future [Publisher: Nature Publishing Group UK London]. *Nature Reviews Earth & Environment*, 1–17. https://doi.org/10.1038/s43017-022-00376-8

Lahann, R., Rupp, J., Medina, C., Carlson, G., & Johnson, K. (2017). State of stress in the Illinois Basin and constraints on inducing failure. *Environmental Geosciences*, *24* (3), 123–150. https://doi.org/10.1306/eg.02061716008170004

Landrø, M. (1999). Repeatability issues of 3-D VSP data. Geophysics, 64(6), 1673-1679. https://doi.org/10.1190/1.1444671

Landrø, M., & Stammeijer, J. (2004). Quantitative estimation of compaction and velocity changes using 4D impedance and traveltime changes [Publisher: Society of Exploration Geophysicists]. *Geophysics*, 69 (4), 949–957. https://doi.org/10.1190/1.1778238

Leetaru, H., & Freiburg, J. T. (2014). Litho-facies and reservoir characterization of the Mt Simon Sandstone at the Illinois Basin–Decatur Project [Publisher:

Wiley Online Library]. *Greenhouse Gases: Science and Technology*, *4*(5), 580–595. https://doi.org/10.1002/ghg.1453

Lumley, D. E. (2001). Time-lapse seismic reservoir monitoring. Geophysics, 66(1), 50-53. https://doi.org/10.1190/1.1444921

MacBeth, C., Amini, H., & Izadian, S. (2020). Methods of measurement for 4D seismic post-stack time shifts [Publisher: Wiley Online Library]. *Geophysical Prospecting*, *68* (9), 2637–2664. https://doi.org/10.1111/1365-2478.13022

MacBeth, C., & Izadian, S. (2023). A review and analysis of errors in post-stack time-shift interpretation. Geophysical prospecting, 71(8), 1497-1522. https://doi.org/10.1111/1365-2478.13391

MacBeth, C., Mangriotis, M.-D., & Amini, H. (2019). Post-stack 4D seismic time-shifts: Interpretation and evaluation [Publisher: European Association of Geoscientists & Engineers]. *Geophysical Prospecting*, *67* (1), 3–31. https://doi.org/10.1111/1365-2478.12688

Meunier, J., Huguet, F., & Meynier, P. (2001). Reservoir monitoring using permanent sources and vertical receiver antennae: The Céré-la-Ronde case study. The Leading Edge, 20(6), 622-629. https://doi.org/10.1190/1.1439008

Miocic, J. M., Gilfillan, S. M., Roberts, J. J., Edlmann, K., McDermott, C. I., & Haszeldine, R. S. (2016). Controls on CO_2 storage security in natural reservoirs and implications for CO_2 storage site selection. *International Journal of Greenhouse Gas Control*, *51*, 118–125. https://doi.org/10.1016/j.ijggc.2016.05.019

Illinois State Geological Survey (ISGS) (2021), Illinois Basin - Decatur Project (IBDP) Geological Models, July 7, 2021. Midwest Geological

Sequestration Consortium (MGSC) Phase III Data Sets. [Dataset]. DOE Cooperative Agreement No. DE-FC26-05NT42588., https://doi.org/10.18141/1854141

Illinois State Geological Survey (ISGS) (2021), Illinois Basin - Decatur Project (IBDP) Seismic Data, July 7, 2021. Midwest Geological Sequestration Consortium (MGSC) Phase III Data Sets. [Dataset]. DOE Cooperative Agreement No. DE-FC26-05NT42588., https://doi.org/10.18141/1854142

Nordbotten, J. M., Kavetski, D., Celia, M. A., & Bachu, S. (2009). Model for CO_2 leakage including multiple geological layers and multiple leaky wells. *Environmental science & technology*, *43* (3), 743–749. https://doi.org/10.1021/es801135v

Onishi, T., Nguyen, M. C., Carey, J. W., Will, B., Zaluski, W., Bowen, D. W., Devault, B. C., Duguid, A., Zhou, Q., Fairweather, S. H., et al. (2019). Potential CO_2 and brine leakage through wellbore pathways for geologic CO_2 sequestration using the national risk assessment partnership tools: Application to the big sky regional partnership. *International Journal of Greenhouse Gas Control*, *81*, 44–65. https://doi.org/10.1016/j.ijggc.2018.12.002

Pevzner, R., Shulakova, V., Kepic, A., & Urosevic, M. (2011). Repeatability analysis of land time-lapse seismic data: CO2CRC Otway pilot project case study. Geophysical prospecting, 59(1), 66-77. https://doi.org/10.1111/j.1365-2478.2010.00907.x

Pörtner, H., Roberts, D. C., Poloczanska, E., Mintenbeck, K., Tignor, M., Alegria, A., Craig, M., Langsdorf, S., Löschke, S., Möller, V., et al. (2022). IPCC, 2022: Summary for policymakers [Publisher: Cambridge University Pres]. https://doi.org/10.1017/9781009325844.001

Ringrose, P., Andrews, J., Zweigel, P., Furre, A.-K., Hern, B., & Nazarian, B. (2022). Why ccs is not like reverse gas engineering. *First Break*, *40*(10), 85–91. https://doi.org/10.3997/1365-2397.fb2022088

Roach, L. A., & White, D. (2018). Evolution of a deep CO_2 plume from time-lapse seismic imaging at the Aquistore storage site, Saskatchewan, Canada. *International Journal of Greenhouse Gas Control*, *74*, 79–86. https://doi.org/10.1016/j.ijggc.2018.04.025

Roelofse, C., Alves, M. T., & Gafeira, J. (2020). Structural controls on shallow fluid flow and associated pockmark fields in the East Breaks area, northern Gulf of Mexico. Marine and Petroleum Geology, 112, 104074. https://doi.org/10.1016/j.marpetgeo.2019.104074

Santos, J. M., Davolio, A., MacBeth, C., & Schiozer, D. J. (2016). 4D seismic interpretation of the Norne Field-a semi-quantitative approach [Issue: 1]. *78th EAGE Conference and Exhibition 2016*, *2016*, 1–5. https://doi.org/10.3997/2214-4609.201601313

Schlumberger Petrotechnical Services (2015). *Time-Lapse 3D VSP Processing Report, Illinois State Geological Survey Illinois Basin – Decatur Project Geophysical Monitoring Well #1, September 2015, 3D VSP Processing* (tech. rep.).

Shipton, Z. K., Evans, J. P., Kirschner, D., Kolesar, P. T., Williams, A. P., & Heath, J. (2004). Analysis of CO_2 leakage through 'low-permeability' faults from natural reservoirs in the Colorado Plateau, east-central Utah. From: BAINES, S. J. & WORDEN, R. H. (eds) 2004. Geological Storage of Carbon Dioxide. Geological Society, London, Special Publications, 233, 43-58. https://doi.org/10.1144/GSL.SP.2004.233.01.05

Stork, C. (2020). How does the thin near surface of the earth produce 10–100 times more noise on land seismic data than on marine data? *First Break*, *38*(8), 67–75. https://doi.org/10.3997/1365-2397.fb2020062

Strandli, C. W., & Benson, S. M. (2013). Identifying diagnostics for reservoir structure and CO_2 plume migration from multilevel pressure measurements. *Water Resources Research*, *49* (6), 3462–3475. https://doi.org/10.1002/wrcr.20285

Strandli, C. W., Mehnert, E., & Benson, S. M. (2014). CO_2 plume tracking and history matching using multilevel pressure monitoring at the Illinois Basin–Decatur Project. Energy Procedia, 63, 4473–4484. https://doi.org/10.1016/j.egypro.2014.11.483

Swager, L. (2019). *ADM CCS1 Injection Well Mechanical Integrity Report March 2019 Pulsed Neutron eXtreme* (tech. rep.).

Williams-Stroud, S., Bauer, R., Leetaru, H., Oye, V., Stanek, F., Greenberg, S., & Langet, N. (2020). Analysis of microseismicity and reactivated fault size to assess the potential for felt events by CO_2 injection in the Illinois Basin. Bulletin of the Seismological Society of America, 110(5), 2188-2204. https://doi.org/10.1785/0120200112

Yang, Z., Xu, T., Wang, F., Yang, Y., Li, X., & Zhao, N. (2018). Impact of inner reservoir faults on migration and storage of injected CO_2. *International Journal of Greenhouse Gas Control,* 72, 14–25. https://doi.org/10.1016/j.ijggc.2018.03.006

Zaluski, W., & Lee, S.-Y. (2021). *2020 IBDP Final Static Geological Model*

Development and Dynamic Modelling (tech. rep.).

Zhang, L., Yang, Q., Zhang, S., Shan, L., Jiang, Q., & Sun, M. (2024). Enhanced CO_2 storage efficiency due to the impact of faults on CO_2 migration in an interbedded saline aquifer. *International Journal of Greenhouse Gas Control*, *133*, 104104. https://doi.org/10.1016/j.ijggc.2024.1

Supporting information for "Carbon dioxide migration along faults at the Illinois Basin – Decatur Project revealed using time shift analysis of seismic monitoring data"

I. Bukar[1], R. Bell[1], A. H. Muggeridge[1], and S. Krevor[1]
[1]Imperial College London, Department of Earth Science & Engineering, London, U.K.

Contents

S1 Feature-based Warping Approach to Time Shift Analysis

We introduce ***Feature-based Warping*** *(FW)*, a modification to Dynamic Time Warping (DTW), which seeks to align matching features (peaks and troughs) in two seismic traces. The dissimilarity error is defined as:

$$\boldsymbol{e_{feature}[i,\, q] = d\big(f_{feature}[i], g_{feature}[i+l]\big)}$$

where $\boldsymbol{f_{feature}[i]}$ and $\boldsymbol{g_{feature}[i+l]}$ are the positions of key features in the baseline and monitor traces, respectively, and $\boldsymbol{d\big(f_{feature}[i], g_{feature}[i+l]\big)}$ is a measure of the distance between the features in the two traces, in this case the L1 or Manhattan distance.

S1.1 Synthetic Modelling

We use well log data from well CCS1 to generate a 1D (pseudo-2D) synthetic model. The well logs are displayed in Figure S1. We select three zones from the RST logs for March 2012 (equivalent to M1) to substitute CO_2; the main injection interval (Mt. Simon A – Lower), a 30-meter interval in Mt. Simon A – Upper, and a 5-meter interval in Mt. Simon C where there is a detection of CO_2 from the RST logs.

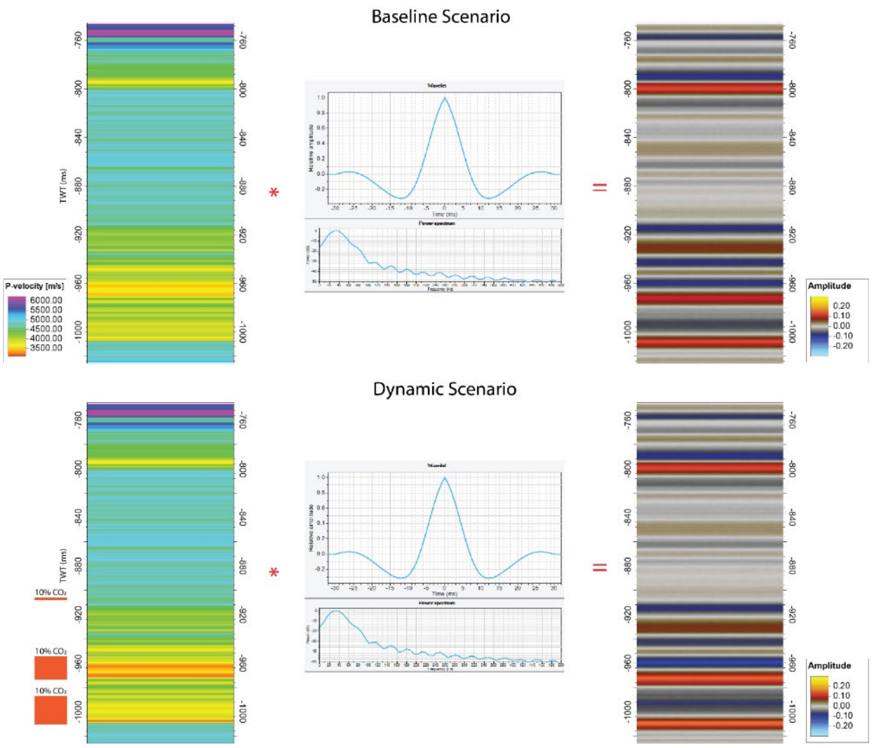

Figure S1: Synthetic modelling based on well log data from CCS1. Baseline and monitor scenarios are produced.

For these zones we choose a 10% CO_2 saturation. Fluid replacement was performed using Gassmann fluid substitution with both fully uniform and patchy mixing to create dynamic or monitor scenarios. The model of acoustic impedance is then convolved with a statistical wavelet extracted from the VSP baseline (B2) so it represents the frequency characteristics in the reservoir region. The same wavelet is used to produce a synthetic seismic for the monitor scenarios. Random noise of 60 dB S/N is added to the outputs. This is shown in Figure S1.

S1.2 Feature-based warping execution

Features (peaks and troughs) are found through a sequential search for local maxima through the traces. Corresponding features are then matched. To avoid cycle skipping challenges caused by spurious features present in one trace but not the other, band pass or low pass filtering may be applied. The features are used to construct a cost matrix where the cost increases with the distance between matched features. The magnitudes of amplitudes of the features are irrelevant. By comparison, the cost matrix for a DTW approach is based on the absolute difference in amplitudes of all pairs of sample points in the traces.

We compare the results of Feature-based Warping (FW), Dynamic Time Warping (DTW), and the true relative velocity change. The feature-based warping approach produces less artefacts and is more efficient as there are less points of comparison. This approach is also able to reliably detect thin layers of CO_2 at low saturations even at lower frequencies, illustrating the robustness of the time shifts detected by this method.

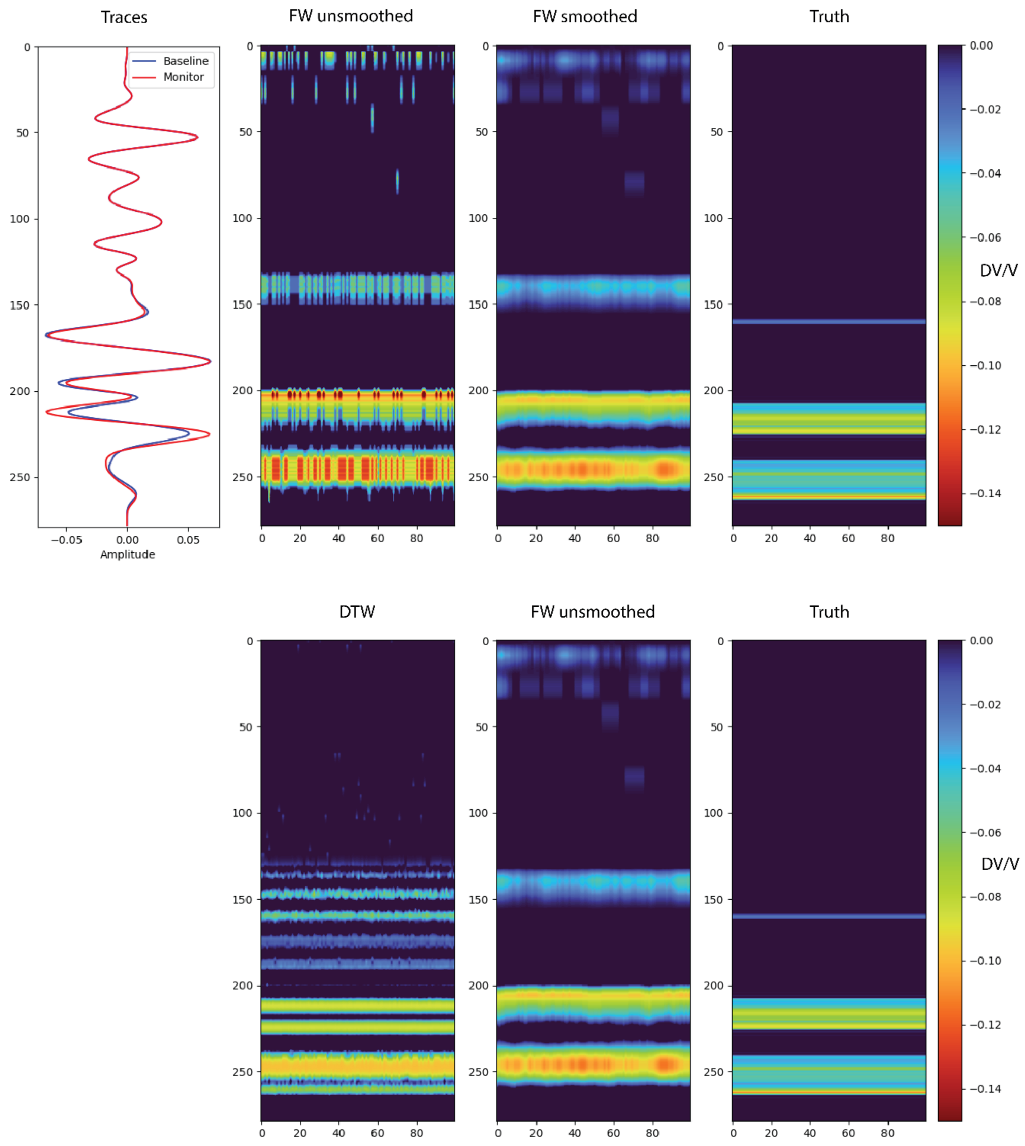

Figure S2: Uniform mixing – Comparison of the feature-based approach with DTW and the true relative velocity change for uniform mixing.

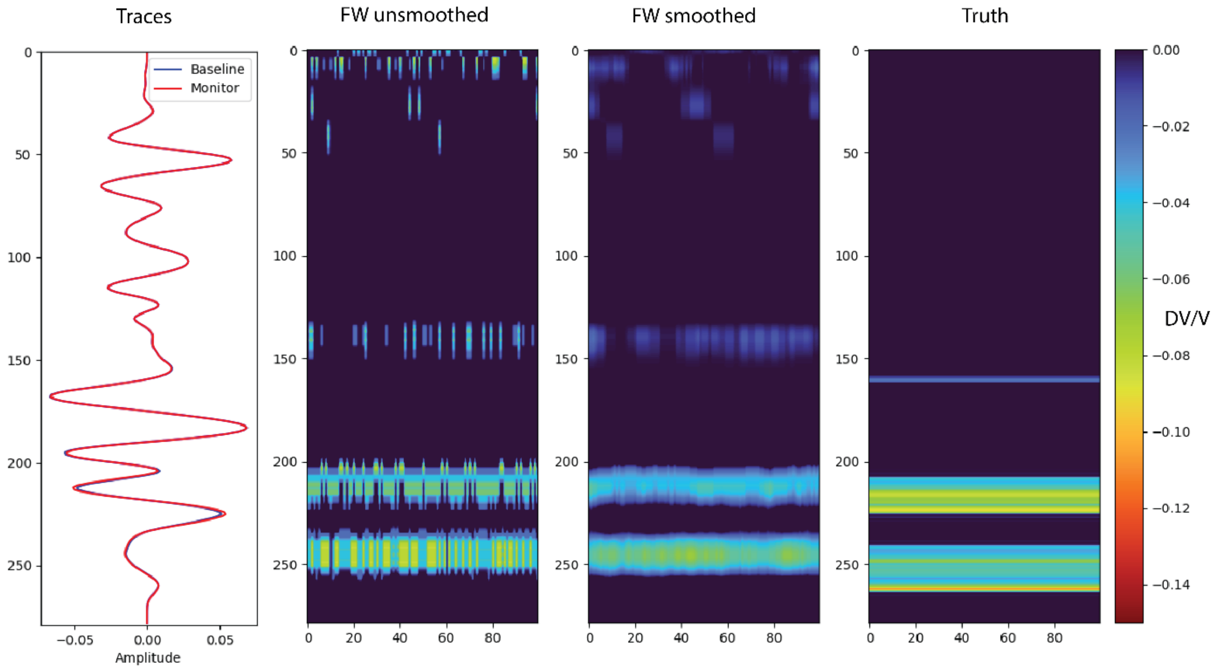

Figure S3: Patchy mixing – Comparison of the feature-based approach with DTW and the true relative velocity change for fully patchy mixing.

S2 Evaluating the possibility of CCS2 as the source of the late CO_2 arrival at injection well post-injection

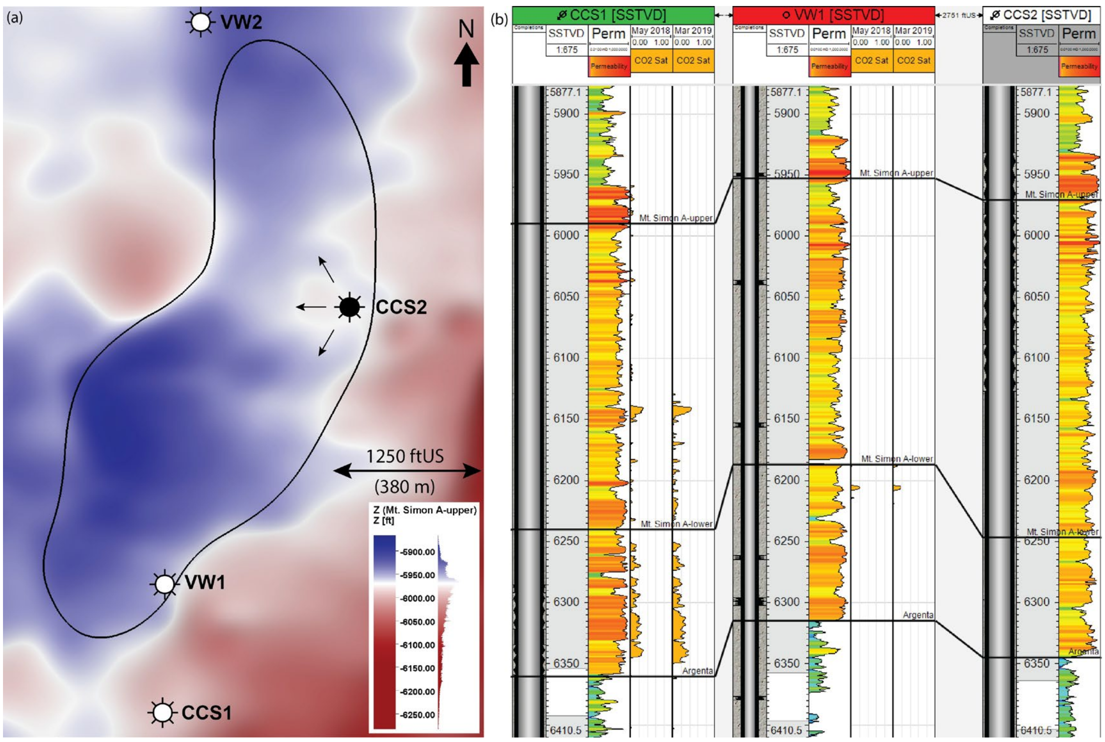

Figure S4: (a) Plume footprint equivalent to 687,000 t of CO_2 derived using a simplified mass and volume balance. We consider flow through only the top one-third thickness of the injection zone at a conservative CO_2 saturation of 0.2 and with no dissolution. (b) Well correlation panel showing wells CCS1, CCS2 and VW1 with no CO_2 detection at VW1.

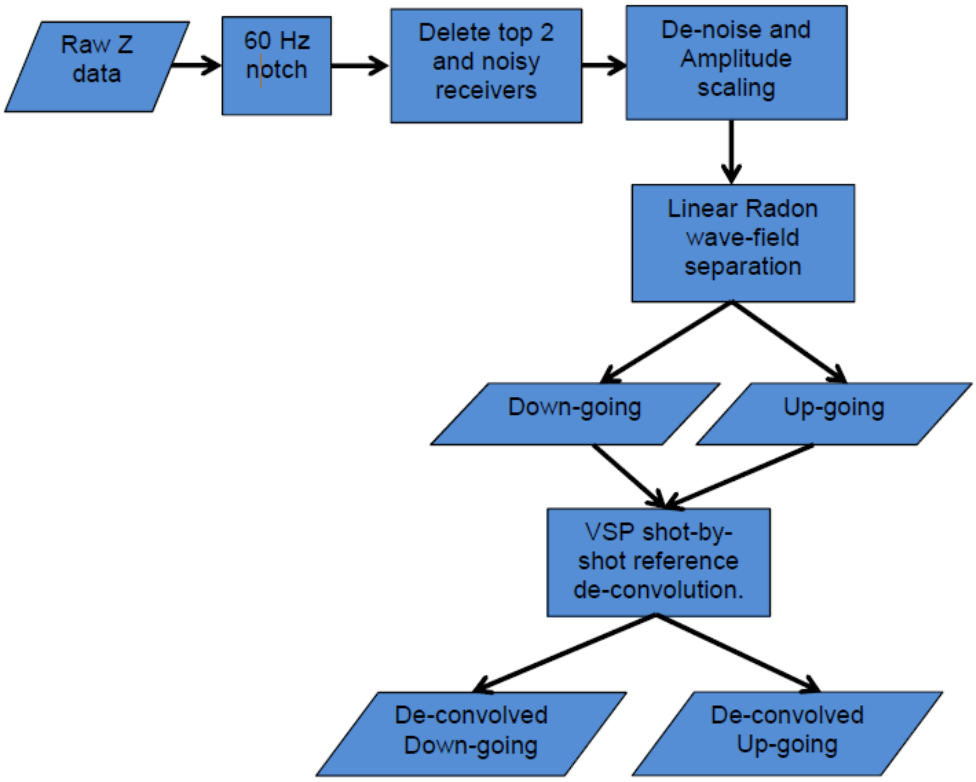

Figure S5: Processing block diagram for 4D VSP data from raw to deconvolution (Schlumberger, 2015).

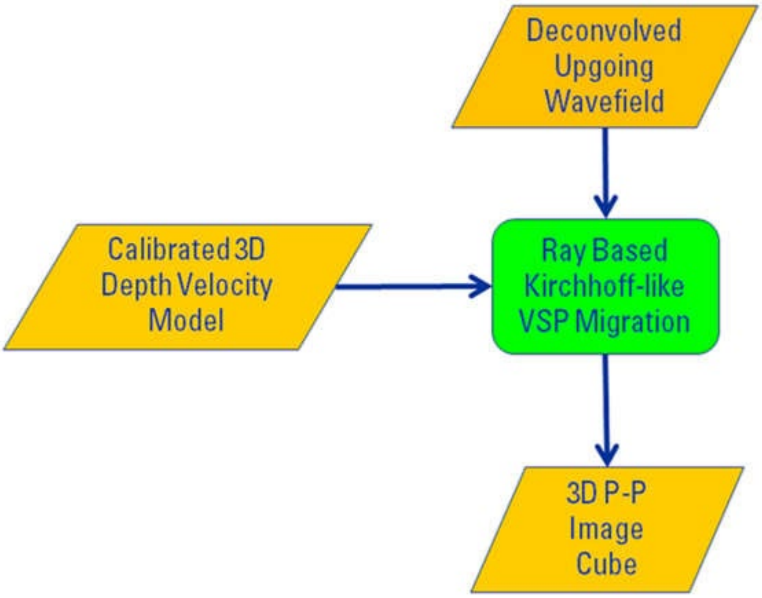

Figure S6: Processing block diagram for depth migration performed on the 4D VSP data (Schlumberger, 2015).

Table S1: Time-lapse VSP survey dates, ground conditions during acquisition and injected CO_2 quantity. Repeated shots refer to the number of shots in the monitor surveys that were co-located with the Baseline 2 survey (i.e., within 50 feet spatial tolerance in source easting and northing coordinates). Co-location issues were encountered due to permit issues with local landowners and the construction of new electrical and industrial infrastructure at the site.

Survey	**Date**	**Ground conditions**	**Vibrator sweep (Hz)**	**Repeated shots (relative to B2)**	**Amount of CO_2 injected (tonnes)**
Baseline 1 (B1)	Jan. 27-30, 2010	Wet	2-100	-	Pre-injection
Baseline 2 (B2)	Apr. 12-14, 2011	Dry	8-120	-	Pre-injection
Monitor 1 (M1)	Feb. 11-12, 2012	Frozen/Dry	8-120	467	74,000
Monitor 2 (M2)	Apr. 4-5, 2013	Damp	8-120	385	433,000
Monitor 3 (M3)	Feb. 3-5, 2014	Frozen	8-120	378	730,000
Monitor 4 (M4)	Jan. 15-17, 2015	Frozen	8-120	458	~1,000,000